Supplementary Information

Plasmonic lithography for the fabrication of surface nanostructures with feature size down to 9 nm

Ping Gao, [a] Mingbo Pu, [a] Xiaoliang Ma, [a] Xiong Li, [a] Yinghui Guo, [a] Changtao Wang, [a] Zeyu Zhao, [a] and Xiangang Luo* [a]

[a] *State Key Laboratory of Optical Technologies on Nano-Fabrication and Micro-Engineering, Institute of Optics and Electronics, Chinese Academy of Science, P.O. Box 350, Chengdu 610209, China.*

* *Email address:* lxg@ioe.ac.cn

1. Numerical simulation of plasmonic lithography in fidelity and contrast

Three-dimension electric fields of plasmonic lithography can be generally obtained according to the vectorial angular spectrum theory [1] [2]. For simplification, here we only concentrate on the two-dimension case, and the electric fields in the photoresist are then represented by:

$$E_x(x,z)=\int_{-\infty}^{\infty}\int_{-\infty}^{\infty}G(k_x)E_x(x,z)T_x(k_x,k_z)\exp(ik_xx+ik_zz)dxdk_x \tag{1}$$

$$E_z(x,z)=\int_{-\infty}^{\infty}\int_{-\infty}^{\infty}G(k_x)E_z(x,z)T_z(k_x,k_z)\exp(ik_xx+ik_zz)dxdk_x \tag{2}$$

where $G(k_x)$ is the illumination function, $E_x(x,z)$ and $E_z(x,z)$ are *x*-direction and *z*-direction electric field components of objects, $T_x(k_x,k_z)$ and $T_z(k_x,k_z)$ are the optical transfer function (OTF) in *x*-direction and *z*-direction. Therefore, for normal illumination ($G(k_x)=1$), the electric field is mainly determined by the OTF $T(k_x,k_z)$.

Subsequently, the OTFs of superlens and cavity lens are investigated. The thickness of the air spacer, top Ag layer and photoresist layer are 10nm, 20nm, and 30nm, which are the same for superlens and plasmonic cavity lens. Different from superlens, there is another 50nm Ag film under the photoresist layer. The complex permittivity of Ag ($-2.168+0.358i$) and photoresist ($2.734+0.11i$) are measured by the spectroscopic ellipsometry. In superlens nanolithography, optical transfer function is $T_{SL}(k_x,k_z)=t(k_x)$ and the transmitted field amplitude $|E_z(k_x)|\propto|t(k_x)k_x|$ is comparable with that of $|E_x(k_x)|\propto|-t(k_x)k_{z,photoresist}|$, where $k_{z,photoresist}=\sqrt{\varepsilon_{photoresist}k_0^2-k_x^2}$ is the longitudinal wave vector in the photoresist layers. In this case, the field would be blurred owing to the phase difference of $\pi/2$. For plasmonic cavity lens with sufficiently thin photoresist, the OTF is expressed as $T_{PCL}(k_x,k_z)=\left[1+r(k_x)e^{ik_{z,photoresist}d_{photoresist}}\right]t(k_x)$, where $r(k_x)$ is the reflection coefficients of the photoresist-silver reflection lens interface. Since the surface plasmon coupling occurs between two silver-photoresist interfaces, which helps to inhibit the negative imaging contribution of E_z, the transmission field amplitude of $\left|E_x(k_x)\right| \propto \left|-t(k_x)(1-r_x(k_x)e^{ik_{z,photoresist}d_{photoresist}})k_{z,photoresist}\right|$ is larger than $\left|E_z(k_x)\right| \propto \left|t(k_x)(1+r_z(k_x)e^{ik_{z,photoresist}d_{photoresist}})k_x\right|$. Therefore, the field tailoring by plasmonic cavity lens helps to improve image contrast and fidelity.

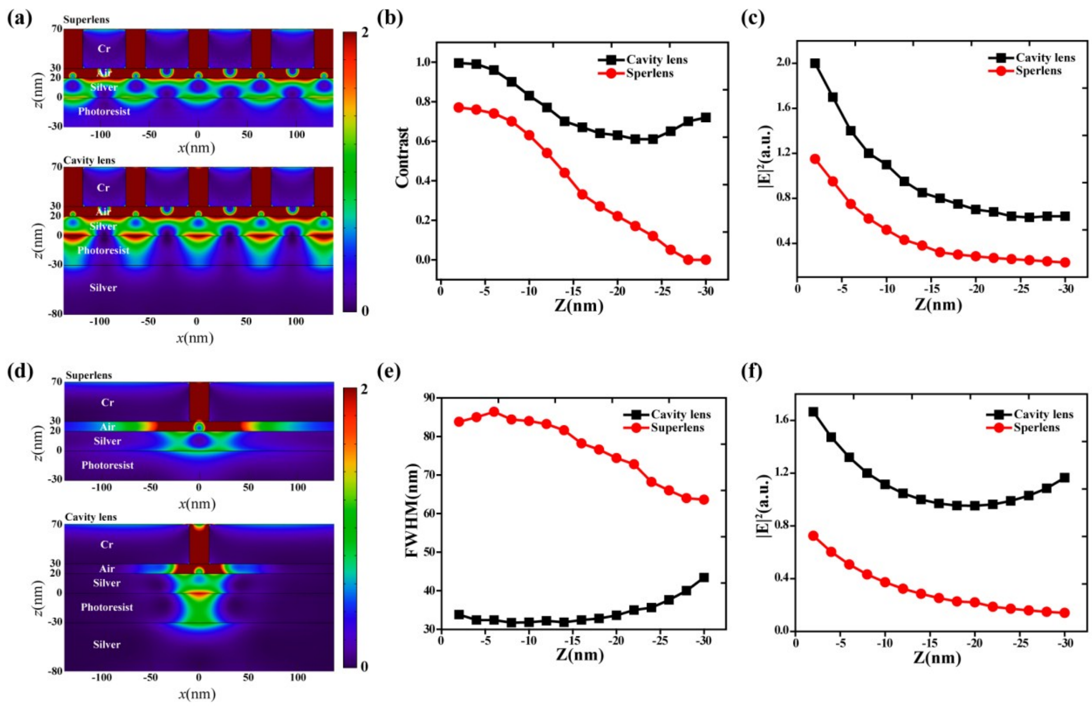

Fig. S1. (a) Electric field intensity distributions of superlens and cavity lens under a normal illumination in the xz plane for density lines. (b) The contrast for variant z positions (horizontal cut lines) in the photoresist of (a). (c) The intensity efficiency as a function of positions along z-axis of (a). (d) The xz plane electric field intensity distributions of isolated structures with normal illumination superlens and cavity lens. (e) The contrast as a function of positions along z-axis of (d). (f) The intensity efficiency as a function of positions along z-axis of (d).

Numerical simulation comparisons are performed to testify the super-resolution lithography model. The thickness and complex permittivity of Cr mask are 40 nm and $-8.55+8.96i$, while others geometries and permittivities are mentioned in OTF calculation. Here, density lines and isolated structures were chosen for our analysis. The period and slit width of density lines were 64nm and 20nm. For isolated structures, the feature size is also 20nm. Figure S1(a) shows the calculated *xz* plane electric field intensity distributions of density lines with normal illumination superlens and cavity lens. Compared to the superlens, there is a strong electromagnetic coupling between two Ag films in cavity lens. Figure S1(b) plots the contrast for variant *z* positions (horizontal cut lines) in the photoresist, where the contrast is defined as $[\max(\left|E^2\right|)-\min(\left|E^2\right|)]/[\max(\left|E^2\right|)+\min(\left|E^2\right|]$. For the contrast criterion of 0.4, the exposure depth of cavity lens is two times larger than superlens, as the additional reflection enhancement of evanescent waves in the cavity lens. This also reflected in the intensity efficiency (Fig. S1(c)). The *xz* plane electric field intensity distributions of isolated structures with normal illumination superlens and cavity lens are given in Fig. S1(d). For numerical analysis, we plot the FWHM of electric field intensity as a function of z position (Fig. S1(e)). The expanding of FWHM can be restrained by cavity lens, due to the significant enhancement of E_x with the plasmonic reflector (bottom Ag film). Anymore, although the FWHM of superlens decrease as z <-6nm, but the electric field intensity efficiency is too small to improve aspect profile. So, the field tailoring by plasmonic cavity lens can improve resolution, contrast, and fidelity, and this can help transfer the pattern onto a thicker polymer resist layer to from core.

2. Pattern shrinkage with initial pitch of 100nm and 88nm

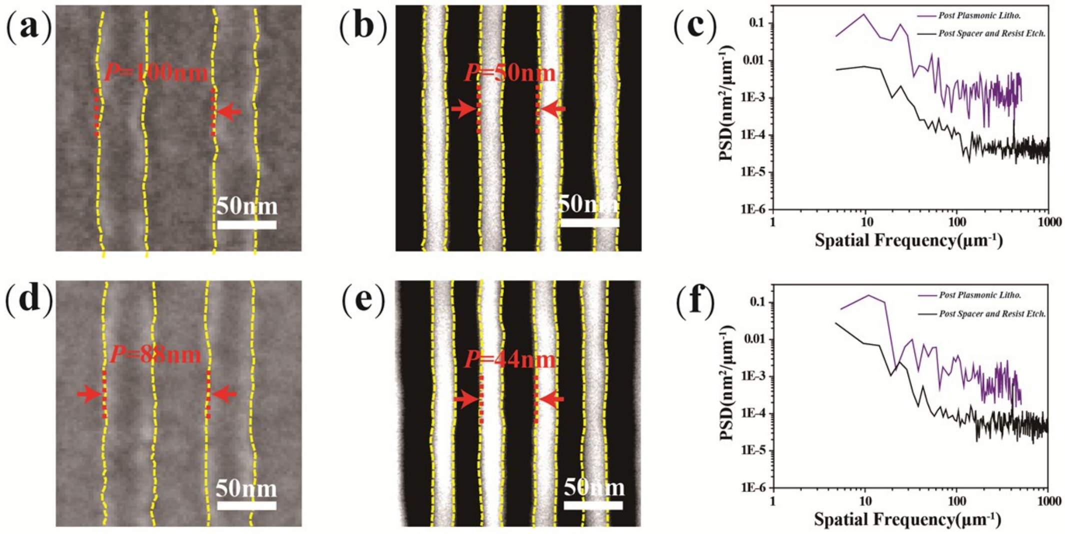

Fig.S2. (a), (c) Top-view SEM images of the post plasmonic lithography results. The pitchs are 100nm and 88nm, respectively. (b), (e) Top-view SEM images of the post spacer and resist etching results for (a) and (c). The pitchs are shrank to 50nm and 44nm, respectively. The yellow dashed lines in Fig. S2(a), (b), (d) and (e) are the skeleton of line edges obtained by SuMMIT. (c) Power spectral density of the LER in Fig. S2(a) and (b). (f) Power spectral density of the LER in Fig. S2(d) and (e).

Figure S2 shows the pattern shrinkage and LER PSD results with initial pitch of 100nm and 88nm. Figure S2 (a), (b), (d) and (e) are the SEM images of the result in the post plasmonic lithography and post spacer and resist etching, which was measured at a local area with ~208×208nm^2. And in these SEM pictures, the yellow dashed lines are the skeleton of line edges obtained by SuMMIT. The LER of plasmonic lithography shown in Fig. S2 (a) and (d) is 6.4nm and 6.0nm, respectively. After the transfer process, spacer and resist etching process, the patterns downscale to the final 50nm (Fig. S2 (b)) and 40nm (Fig. S2 (e)) pitch grating patterns. And the LERs are also gradually reduced as the patterns scaling, down to 1.5nm and 2.0nm, respectively. As shown in Fig. S2 (c) and (f), the middle and high spatial frequency regions from 6μm^{-1} to 1000μm^{-1} contribute most to the overall LER reduction.

References

1 Xiangang Luo, Principles of electromagnetic waves in metasurfacces, Science China Physics, Mechanics & Astronomy, 2015, 58, 1-18

2 Xiangang Luo, Mingbo Pu, Xiaoliang Ma, Xiong Li, Taming the electromagnetic boundaries via metasurfaces: from theory and fabrication to functional devices, Int. J. Antennas. Propag. , 2015, 2015: 204127